



Numerical analysis of heat transfer in helical tube with the aluminum oxide Al_2O_3 nanofluid injection in water

Hamid Zalnezhad^a, and N. Kordani^{b,*}

^aDepartment of Mechanical Engineering, Islamic Azad University, Nour Branch, Nour, Iran.

^bDepartment of Mechanical Engineering, University of Mazandaran, Babolsar, Iran.

Article info:

Type: Research
Received: 25/06/2018
Revised: 12/05/2019
Accepted: 25/05/2019
Online: 26/05/2019

Keywords:

Nanofluid,
Helical tube,
Injection in wall,
Heat transfer.

Abstract

The most important reason for the design of curved tubes is increasing the heat transfer between the fluid and the wall, which has provided many applications in various industries such as air conditioning, micro-electric, heat exchangers and, etc. The aim of this study is a numerical investigation of nanofluids flows in spiral tubes with an injection of base fluid in different Reynolds numbers. The effects of volume fraction, nanoparticle diameter, fluid injection, Reynolds number, and spin effects on heat transfer and flow in the spiral tube are discussed. In this study, a mixture of water- Al_2O_3 is selected to model nanofluid flow in order to investigate the changes in the heat transfer rate by the injection of nanofluid to the base fluid in the spiral tube at different angles. The results show that by the use of nanoparticles, the rotational effects of the tube and the injection process increase the heat transfer performance. It is found that increasing the volume fraction has a direct effect on increasing the heat transfer coefficient. As the volume fraction increases from 2% to 8%, the heat transfer coefficient increases by 2%. In fact, the effect of nanoparticles on the thermal conductivity of the fluid causes this increase. Also, injection of fluid into the stream due to disturbance in the thickness of the boundary layer and the further mixing of the fluid layers which increases the heat transfer. The 90-degree injection has the best effect. Cu_2O_3 -water nanofluid mixture is also used. The results and the comparison with the Al_2O_3 nanofluid model indicate that the increase in heat transfer rate in Cu nanofluid is higher than aluminum nano fluid due to higher heat transfer capacity of copper.

1. Introduction

The increase in thermal transfer has always been an important issue in the industry. There are many methods of increasing thermal transfer without increasing the weight and dimensions of the converter. Using these methods in industries, such as electronics and space, the design and manufacture of thermal converters with small

dimensions, light weight, and high efficiency is necessary. For increasing the thermal transfer, changing the geometry of flow, boundary condition, and increasing fluid thermal conductivity can be used. Because of the limitations of the flow geometry and boundary conditions, the best option for researchers is increasing fluid thermal conductivity. For this reason, this method has been widely studied.

*Corresponding author

email address: naser.kordani@umz.ac.ir

However, the low thermal conductivity of the fluids is a common factor in thermal equipment such as water, engine oil, ethylene glycol, which is the primary limitation for development of these equipment. It is well cleared that metals have much high thermal conductivity than fluids. For example, copper's thermal conductivity at room temperature is almost 700 times of water and 3000 times of engine oil. Because of this reason, it is expected that fluids with solid suspended metallic particles or metallic oxide have more thermal conductivity than pure fluids.

The idea of putting small metallic particles inside fluid for increasing thermal ability was presented by Maxwell about a century ago. But until the past few years, investigations have only been carried out on particles with a millimeter or micrometer size. In these scales, because of largess of the particles, in addition to low thermal efficiency, problems such as fast settlement, creation of trituration in the flow path, corrosion, and enhancement of pressure anticlimax have been seen. With the development of nanotechnology and nanosized particles, nanofluids are a new generation of fluids that contain nanosized particles and can overcome these problems by helping to create a sustainable suspension.

Thermal transfer efficiency "h" increases in curved tubes with the increase in Dean Number

$De = Re \sqrt{\frac{D_h}{R}}$. In fact, in direct tubes, the Nusselt number stays constant. In the above equation, Re is the Reynolds number, R is the curve radius, and D_h is the tube's hydraulic diameter. The maximum rate of Nusselt number in curved tubes also reported to 10 times more than that of direct tubes. This increase in the thermal transfer coefficient can be related to two mechanisms. First, centrifugal force arising from curvature of the tube causes some sorts of secondary whirlpool flows to appear in curvature location that this is the main reason for increased thermal transfer. Second, flow in curved tube cannot be considered like direct tubes. It is well cleared that h in the thermal entrance length is more than in thermal developed area [1-7].

As mentioned before, nanofluids show extraordinary specifications in thermal transfer

in comparison with common fluids that can impressively improve fluid's thermal and mechanical performance [8-11]. The most important and fundament possible reasons are as following:

- Suspended nanoparticles cause surface area and thermal capacity of fluid to increase [12].
- Suspended nanoparticles cause fluid's efficient thermal conductivity to increase.
- Internal interactions escalate with tilting between particles, fluid, and surface of passing flow [13].
- Mixed oscillations and fluid's collision escalate.
- Nano particles dispersion makes the fluid's temperature gradient more uniform. Nano particles increase thermal transfer rate with increasing the thermal conductivity of nanofluids and impose the thermal dispersion in the fluid and it is a new way of increasing thermal transfer process [14-22].

Resistance in boundary layers of transfer processes has a huge effect on transmission rate, so if in a method, the thickness of this layer decreases, an impressive improvement in increasing mass transfer, temperature, and momentum transfer will result. One of the nearly modern methods related is using impinging jets. In this method, applying a significant momentum to an output fluid from nozzle and its collision with the desired surface in the process cause a disturbance in the boundary layer, and the resistance to transmission decreases. Impinging jets have a lot of applications in the industry which can be pointed as follows:

- In cooling processes such as cooling chemical and nuclear reactors, cooling gas turbine blades, and cooling electronic pieces.
- In flaming and combustion heating processes such as direct contact of combustion gases with furnace housings (recently significant research has been started on the development of new methods of combustion in the form of impinging jets).
- In drying processes in the medical and food industries, the textile industry, and paper manufacturing industries.
- In coating processes and coating technology, with chemical vapors deposition method,

such as the production of thin industrial diamond film.

- In shear, erosion and corrosion processes such as cutting technology with water or investigation of erosion phenomenon caused by jet encounter to surface.
 - In heating-cooling processes with shaping, like glass-making industries and producing metal sheets.
 - In the technology of vertical flight airplanes.
- Considering the reasons given above, in the ability to imping jets in the failure of the boundary layer and shifting the molecular penetration transfer to forced displacement, impinging jets bring one of the fastest thermal transfer methods. Because of the complexity of the mechanism, usually, information about thermal transfer coefficients of impinging jets is not available in common sources, references, and thermal transfer handbooks or equations, and quantities presented are mostly for special researched systems that are not fully applicable. So this subject is the topic of the research day in the world. The importance of impinging jets and their effect on flow square structure is too much. So, how the behavior of the return flows and vortices resulting from them, as well as the fluid accumulation in the path of the jets, can have a significant effect on heat and mass transfer coefficients.

According to the terms given above, it is expected that by using every three methods given above contemporary, an impressive increase in the thermal transfer can be seen. To examine this subject, the curved tube with the curvature of 90° with constant temperature in the wall and the fluid water, will be considered. Spherical particles of aluminum oxide (Al_2O_3) flow as the nano-sized particles within the tube and water are injected through the wall.

Xuan and Li [23] examined the thermal transfer of the turbulent nanofluid displacement inside the tube, and they observed that the thermal transfer displacement coefficient increases with increasing flow velocity and volume percent. Y. They expressed in another research [24] that thermal transfer incensement happens until a particular volume percent of the nanofluid, and after that, because of increasing viscosity, the increase in thermal transfer stops. For this

reason, choosing the right volume fraction of nanoparticles for increasing thermal transfer should be done with accuracy. In another study, Sheikhzadeh et al. [25] solved the momentum and energy equations of laminar flow of a non-Newtonian fluid in an axisymmetric porous channel using the least square and Galerkin methods. In this study, the effects of Reynolds number, Prandtl number, and power law index of the non-Newtonian fluid are examined on the flow field and heat transfer. The results show that the Nusselt number increases by increasing the Reynolds number, Prandtl number, and power-law index. In the design of heat exchangers, it is necessary to determine the heat transfer rate between hot and cold fluids in order to calculate the overall heat transfer coefficient and the heat exchanger efficiency. Mazidi et al. [26] estimated the unknown space-time dependent heat flux imposed on the wall of a heat exchanger internal tube by applying an inverse method and simulated temperature measurements at the specified points in the flow field. Results show that the variable metric method is a rapid and precise technique for estimating unknown boundary conditions in inverse heat convection problems.

Fotokian and Nasr Esfahany [27] investigated forced thermal transfer displacement of non-regular nanofluid flow of water- Al_2O_3 experimentally. They examined the inside of the tube and showed that thermal transfer coefficient increases about 35% in compared with pure water. Zeinali et al. [28] researched the experimental study of the thermal transfer of free displacement of water- Al_2O_3 nanofluid in a channel with a square-cross section. The flow was calm, and walls had constant thermal flux. Shedid [29] computed the thermal behavior of the nanofluid in a circular tube. His under investigation model was disturbed, and the walls were at a constant temperature. Nanofluids used was Al_2O_3 and Ti_2O_3 with water. Choi and Zhang [30] carried out a simulated thermal transfer of the pacific forced displacement thermal transfer of water- Al_2O_3 nanofluid into a tube with a bend of 180° using finite element method (FEM). The effects of the secondary flow on the thermal transfer inside the bend were investigated. Xuan and Li [16] examined the drop-in pressure and

convective heat transfer of water and nanofluids in a double-housed helix thermal converter.

The aim of the present study is a numerical investigation of nanofluids flow in spiral tubes with an injection of the base fluid in different Reynolds numbers.

2. Method

2.1. Numerical solution method

As mentioned earlier, numerical analysis is done using Fluent software, and Navier-Stokes equations are solved by means of commercial code. This software uses the limited volume method in which the computational domain breaks into a series of elements. This is done by using mesh production software like GAMBIT. Then, the decomposition algorithms on density-basis for solving the governing equations for the survival of mass, momentum, and energy and other scalars such as confusion within control volume are used.

Nanofluid simulation has been based on one phase and obtained nanofluid specification using valid empirical and numerical formulas.

In the following equations φ is the contraction coefficient, W is the volume fraction, ρ_f is the water density, and ρ_p is the nanoparticle density. The equations are achieved for computing specification of nanofluids by Maxwell. Density of nanofluid is as follow:

$$\rho_{nf} = \varphi\rho_p + (1 - \varphi)\rho_{bf} \tag{1}$$

Thermal capacity of nanofluid is measured using Eq. 2, as follow:

$$C_{p_{nf}} = \varphi\rho_p C_{p_p} + (1 - \varphi)\rho_{bf} C_{p_{bf}} / \rho_{nf} \tag{2}$$

Dynamic viscosity of nanofluid can be obtained using Eq. (3).

$$\mu_{nf} = \mu_{bf} \exp \left[\frac{4.91\varphi}{0.2092 - \varphi} \right] \tag{3}$$

Thermal conductivity of nanofluid is calculated using Eq. (4).

$$k_{nf} = k_{bf}(1 + 4.5503\varphi) \tag{4}$$

Although other valid equations such as Williams and others published for computing nanofluids properties, the values are all close to each other. Considered volume fraction is 7.04 percent, and its volume concentration coefficient is 1.88 percent. Table 1 shows the specification of the base fluid and nanoparticles. For simulating nanofluid's flow, used fluid, base fluid of water, and nanoparticles of Al₂O₃, the spiral tube is made of copper. First, in some cases, the model is verified with experimental data [28] and valid papers. Initially, the geometry of valid articles is modeled and analyzed with Fluent software, and the effect of changing geometric parameters is investigated. The boundary condition of the solution is also analyzed with the thermal transfer rate, and the boundary of the constant temperature wall is compared.

Numerical analysis is done using a commercial software named Fluent which is the software of fluids analysis. For simulation, first, the model drawn up in design software. In the next step, this model enters to Fluent software and it is analyzed after entering boundary layer quantities and determining the solution method. Simulation done by simulator software has special levels that should be run step by step until the end, and intended results are achieved. The levels are respectively as follows:

1. Producing desired geometry
2. Meshing
3. Applying boundary conditions or primary conditions.
4. Solving using numerical methods

To ensure the simulation and validation of results, experimental and numerical published results in the field of nanofluid in spiral tubes are used. From valid works in this field, the experimental model that has been used in references [31-34] can be named.

Table 1. Specifications of different phases in 90° connection with nanofluid.

Solid phase (aluminum oxide)	Fluid phase (water)	Specifications
880	4182	C _p (j/kg k)
3920	998	ρ (kg/m ³)
-	0.001003	μ (kg m ⁻¹ s ⁻¹)
40		dp (nm)

2.2. Geometry production

The geometry drew in SolidWorks software, is shown in Fig. 1.

2.3. Mesh geometry

GAMBIT 2, 4 software is used to create the grid. This software has the ability to create an unstructured and organized mesh. The simplest type of grid is an unorganized mesh that generates a mesh of unstructured elements by generating triangular elements on geometry surfaces and producing elemental elements in blocks. Fig. 2 shows 520,000 generated mesh. It contains cube-size elements.

Because of the importance and effect of adjacent cell walls on the results, it is essential that the elements adjoin the tube wall, and are tiny enough. To do this, the boundary layer mesh is used.

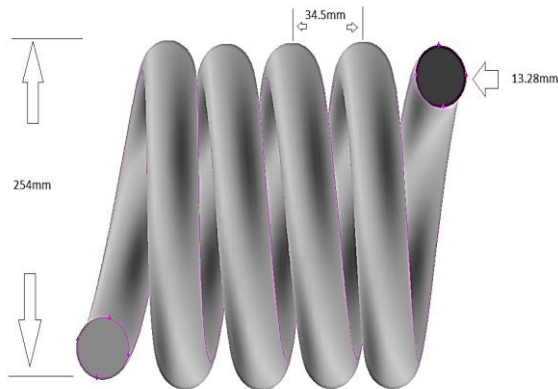


Fig. 1. Spiral tube.

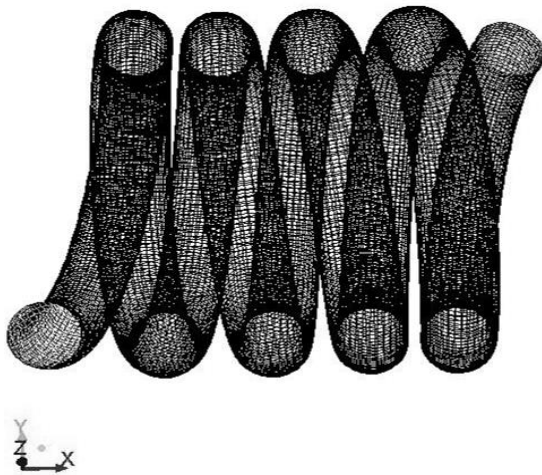


Fig. 2. Created mesh for spiral tube.

To use this type of mesh, the height of the first layer near the wall is adjusted, and the next elements with the appropriate growth rate are created.

Fig. 3 shows an overview of the boundary layer mesh in tube inlet. As can be seen, adjacent cells in the borderline mesh are close enough to the wall. The height of the first layer is 0.08 millimeter, and numbers of layers are 12, and the growth rate of the layers is 1.2. The Total height of the boundary layer is 3.166 millimeters. The correctness of the height and size of the first layer is determined by the parameter named y^+ .

2.4. Mesh independency

To solve the problem, independent of the number of grid elements, the influence of this parameter is investigated. Thus, the velocity parameter at the end of the tube is investigated in meshes with a number of different elements. As shown in Fig. 4, the number of elements with the number of greater than 500,000 in the tube show the mesh independence.

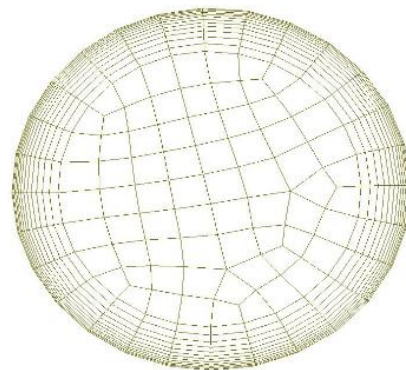


Fig. 3. The boundary layer mesh produced at the entrance of the spiral tube.

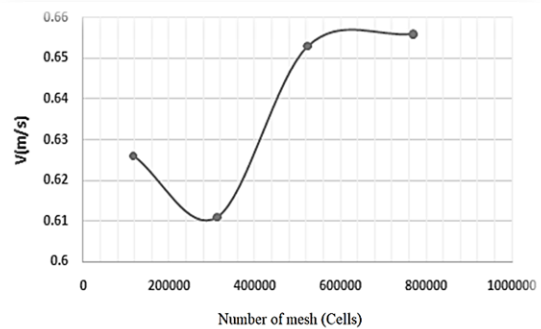


Fig. 4. Velocity vs. number of mesh.

2.5. Boundary conditions

Boundary conditions contain flow inlet and flow outlet. Tube's and nanofluid's temperatures of 293 K and 301 K are considered.

3. Results and discussion

GAMBIT 2.4 is used to create the mesh for geometry with injection. Fig. 5 shows an overview of the mesh generated in GAMBIT software. This software has the ability to create both unorganized and organized meshes. The simplest type of meshes is the unorganized one, which generates unorganized elements by producing triangular elements on the geometry surfaces and the production of prismatic elements in the blocks. Another type of mesh is the production of rectangular elements on the surface, and finally, the production of rectangular cube-shaped elements. The generated mesh is a combination of square and irregular elements. The reason for this irregularity is related to geometry.

Due to the importance of the near-wall elements of the tube and the impact of the meshes quality of this area on the results, the boundary layer mesh is produced (Fig. 6).

To solve the problem, independent of the number of elements of the mesh, the effect of this parameter is researched. Thus, the velocity parameter at the end of the tube is investigated in meshes with different number of elements.

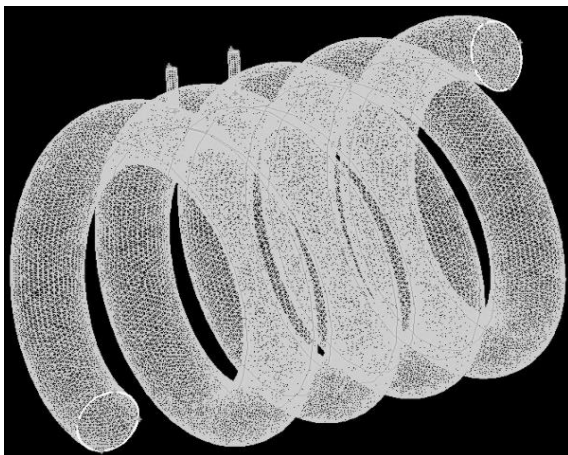


Fig. 5. Meshing of a three-dimensional tube with injection.

Fig. 7 shows the friction coefficient as a function of mesh number. The values are the mean of the friction coefficients for the whole tube. This diagram shows that the system, after selecting a value for the initial assumption, performs the calculations in the corresponding formula, and each time the number of elements increases. The calculation accuracy increases and eventually reaches a constant value in the number of elements of 1.500.000. As shown in Fig. 8, the number of elements, more than 1,500,000 inside the tube, represents the independence of the mesh. Fig. 8 shows the output velocity at the tube's outlet cross-section. For different sections of the tube, the form of convergence and the amount of quantities is similar to that of the same figure. By increasing the mesh, due to the closer coverage of the cells in adjacency, the velocity values at a point in the tube are calculated more accurately. This also applies to the coefficient of friction at the tube surface.

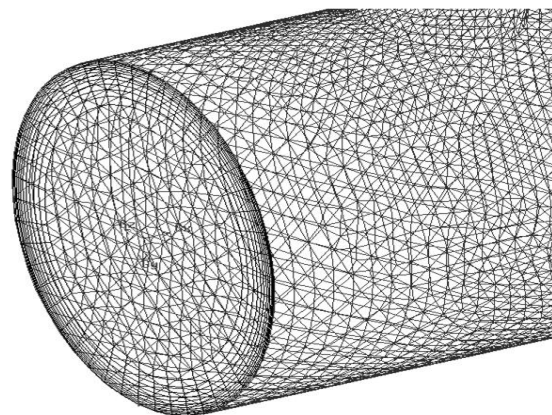


Fig. 6. Boundary layer mesh generated at the entrance.

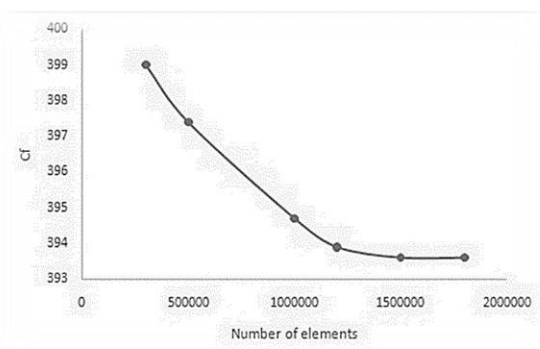


Fig. 7. Friction coefficient values vs. mesh number.

In Fig. 9, the graph of thermal transfer coefficient as a function of Reynolds number, which is taken from references [28-31], can be seen. In this figure, amounts are brought in six different volume fractions (water, 0.78%, 2.18%, 3.89%, 5.68%, and 7.04%), and results are until Reynolds number of 9000.

Figs. 10 and 11 show amounts of thermal transfer coefficient and its comparison with experimental results in nanofluid with purity percentages of 2.18%, 3.89%, and 7.04% in different Reynolds numbers. The numerical solution is done for fluid of water and nanofluid using a single-phase method. In laminar flow (Fig. 10), numerical amounts show the correctness of the method in this article. In laminar flow, the numerical amounts are less than 3% of error in comparison with experimental data. When Reynolds number passes from 6000-6500, because of changes in flow conditions, by increasing Reynolds number, the numerical values are far from the experimental values, which indicates a greater error.

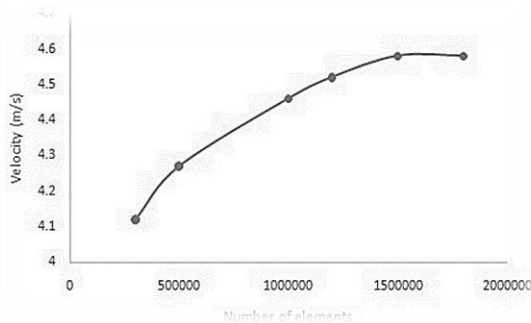


Fig. 8. Output velocity values vs. mesh number.

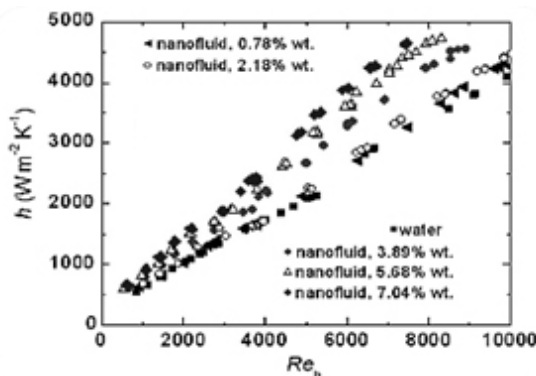


Fig. 9. Thermal transfer coefficient vs. Reynolds number from reference.

For the Reynolds numbers above 6000, flow is turbulent (Fig. 11), and the average error in the turbulent area is about 5 %, and totally there are two steady flows with an error percentage of fewer than 4. Similarly, by examining and extracting the data obtained in simulation, and comparing the data with experimental data, one can conclude that the method of carrying out the work with a very small margin of error with the method of performing empirical work, it is the same, and the work is continued.

After making sure of the work method, the review of the work step by step and analyzing the result of each section are done.

Fig. 12 shows the locations of the plates created on the spiral tube mesh. These plates are designed to compare the results of the analysis in each tube bend.

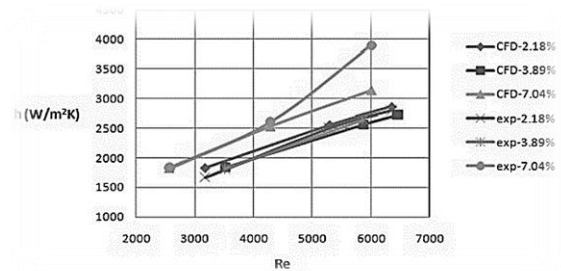


Fig. 10. Heat transfer coefficient vs. Reynolds number for laminar flow.

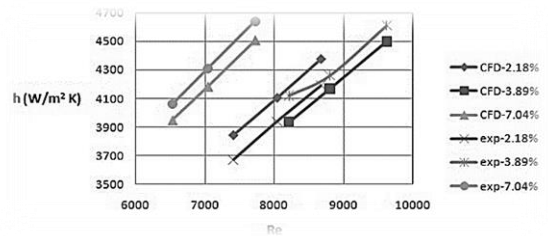


Fig. 11. Heat transfer coefficient vs. Reynolds for turbulent flow.

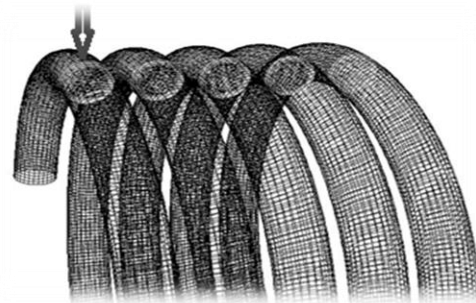


Fig. 12. Created plates on the mesh are shown in the cross section.

Fig. 13 shows the amounts of pressure in the spiral tube in the first to fifth bend for speed of 0.4 m/s. Velocity inlet is from the left side that the red color of the figure shows the tube's first bend. The pressure drop is well shown in the tube. As can be observed, due to the existence of the return area, the velocity near the inner wall of the tube is negative, and the maximum speed is toward the outer wall of the tube. But, by moving the path, velocity changes move toward the inner wall and because of the reverse pressure gradient and the separation of the boundary layer, a return area forms after a 45° angle, and vortices are formed near the inner wall of the tube.

By analyzing the above process, the results are achieved, and the temperature decreases with moving the path along the tube. So, by applying new conditions, the thermal transfer speed increases, and it is controlled to some extent. It should also be pointed out that when the speed issue divides the velocity inside the tube, the thermal transfer by tube wall and water with the environment around increases (Figs. 14 and 15).

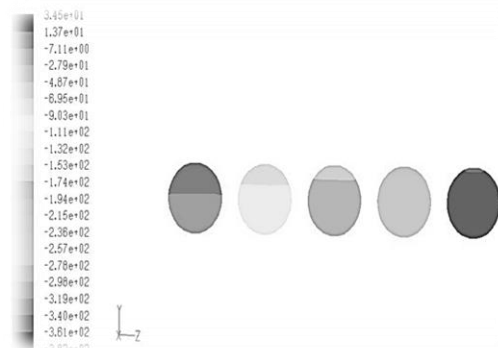


Fig. 13. Pressure in the spiral tube in the first to fifth bend for speed of 0.4 m/s.

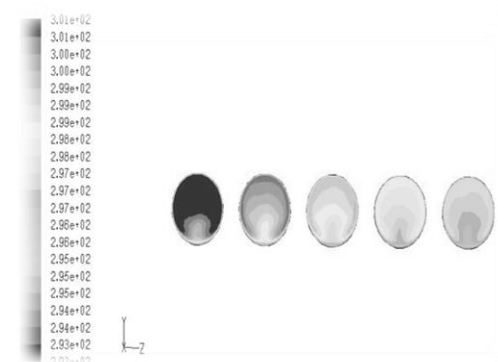


Fig. 14. Temperature in the spiral tube in the first to fifth bend for speed of 0.4 m/s.

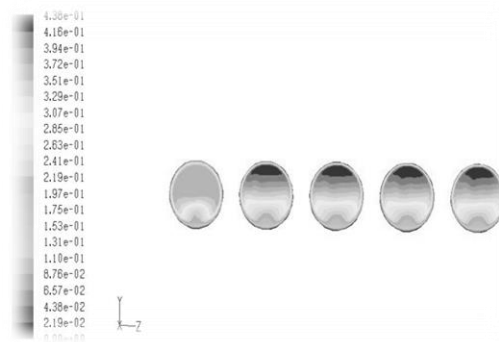


Fig. 15. Velocity in the spiral tube in the first to fifth bend for speed of 0.4 m/s.

Fig. 16 shows the view of the connection tube and injection sites. In this section, the simulation of the nanofluid flow inside a spiral tube with injection into the tube is worked on. The dimensions of the tube are the same as before. In this geometry, the injection injects from two parts of the tube into the tube. There are three different considered states of injection for the tube.

Figs. 17 and 18 show the velocity distribution for the symmetry geometry. As it is seen, the velocity decreases in areas close to the injection and increases in the tube bending area. The increase in velocity after passing through the bend rises. As shown in Fig. 17, the presence of turbulence, caused by fluid injections, is the cause of the velocity decrease in the injection area. In order to better investigate the effect of injection in different positions, two injections on the tube are considered in different positions. Fig. 19 shows the amounts of injection in the longitudinal section of geometry. As can be seen, by the injection, the velocity distribution in the tube is cluttered.



Fig. 16. Three-dimensional tubes with injection.

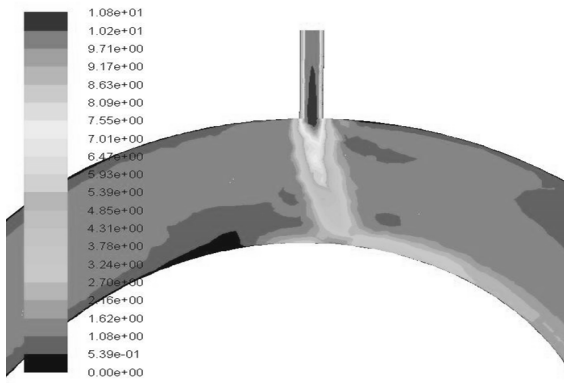


Fig. 17. Distribution of velocity for symmetry plate.

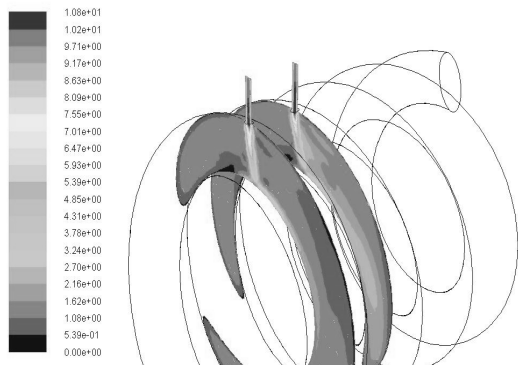


Fig. 18. Distribution of velocity for two injections on the symmetry plate.

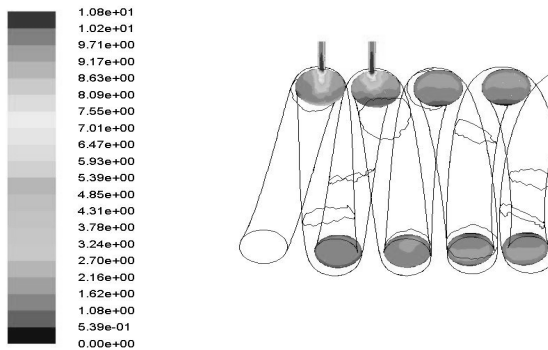


Fig. 19. Distribution of velocity on the middle plate.

In Fig. 20, the distribution of temperature on the tube is observed for two parallel injections. As a result of the injection, fluid's clutter is led to an increase in the thermal transfer of the injection areas.

In Figs. 21 and 22, the velocity distribution in the 90° injection is observed on the tube, which is more uniform for the injection in a 90° mode of flow distribution in the whole tube. This is due to the intensity of turbulence in Fig. 23. By

injection of turbulence, the injection site increases and the turbulence is added to the flow inside the tube and increases the heat transfer rate.

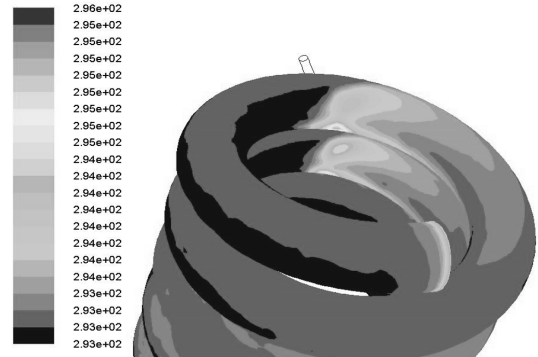


Fig. 20. Distribution of temperature on the tube for two parallel injections.

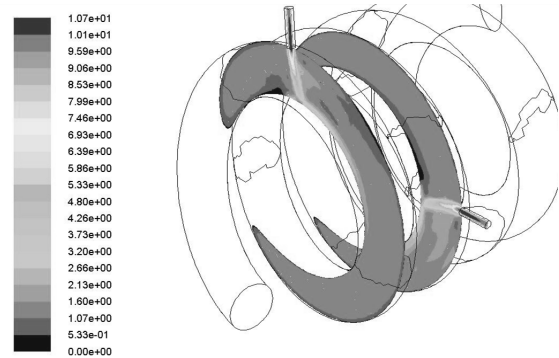


Fig. 21. Velocity distribution in 90° injection on the tube.

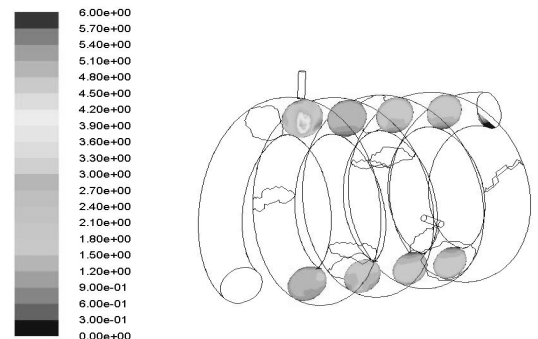


Fig. 22. Velocity distribution of middle plate in 90° injection on the tube.

In Fig. 24, the next injection mode on the tube is seen in a double injection mode with a 180° angle. The velocity distribution in this mode is given for the middle plate. The velocity values have a more normal distribution than the other two modes.

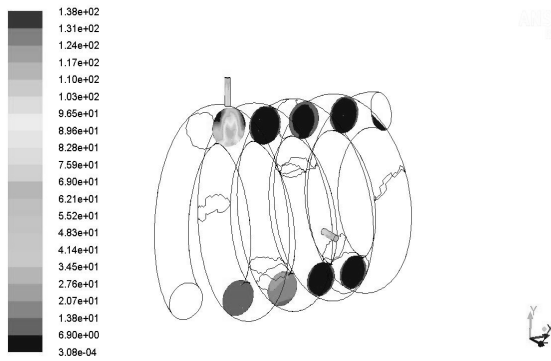


Fig. 23. The amounts of turbulence intensity of middle plate in 90° injection on the tube.

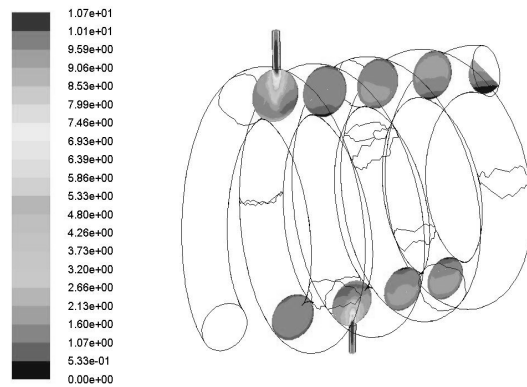


Fig. 24. Velocity distribution of middle plate in 180° injection on the tube.

For the better investigation, the turbulence intensity on the middle page is shown in Fig. 25 for a 180° mode. Comparing the amounts of the intensity of turbulence, it is observed that the effect of injection in the next periods of injection rapidly disappears. This is because of the long interval between the two injections that the continuous effect of the injection is lost. The Ansys software can extract various thermal transfer coefficient data in different points of geometry at output data (Fig. 26).

This amount of thermal transfer coefficient is obtained by dividing the amount of energy transferred into the temperature difference created on the surface and position. So, if a line is drawn on the geometry and the wall, the values of changes in the thermal transfer rate can be seen. Also, the calculation of the software is based on the average thermal transfer rate or Nusselt number on the entire geometry.

In the following analyzes, two injections with a 90° angle are investigated to examine two different velocity injections. In one mode, the second injection rate is 50% less than the first injection, and in another case, the second injection rate is 50% higher than the first injection rate. The results show that, due to the increase in the second injection rate, the heat transfer rate compared to the two-injection mode with a velocity equals a slight increase of about 0.5%. The rate of reduction has a more significant effect on the transmission rate and has reduced by about 1.5% of the heat transfer rate. Table 2 presents the values of various analysis data. The heat transfer rate is compared to the non-injection mode.

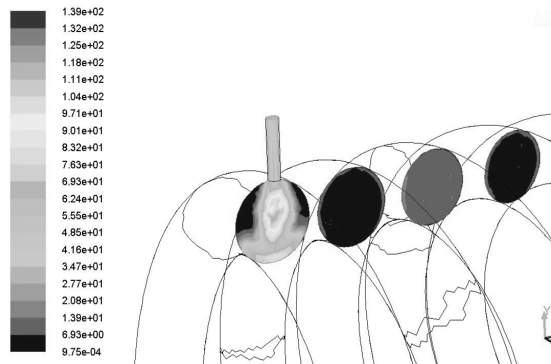


Fig. 25. The amounts of turbulence intensity above the middle plate in 180° injection on the tube.

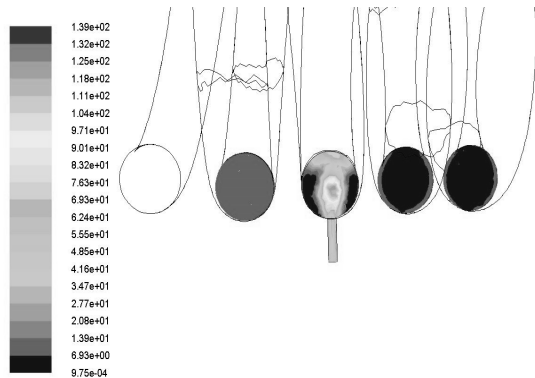


Fig. 26. The amounts of turbulence intensity down of the middle plate in 180-degree injection on the tube.

3.1. Investigation of Reynolds effect

To investigate the effect of Reynolds number, the numerical solution is performed at velocities of 2, 3, and 5 m / s. The Reynolds number range of the current study is from 4393 to 10982. From the study of nanofluid flows inside the tube, it

appears that the flow with the Reynolds number values below 6000 is a steady flow [35]. The values of the thermal transfer coefficient in Reynolds number are the same as shown in Fig. 27. As can be seen, increasing the Reynolds number increases thermal transfer due to the increased kinetic energy of particles. It increases the friction of the flow with the tube, which is itself an agent in order to increase the thermal transfer coefficient. All analyzes are for 90° injection mode.

Fig. 28 shows the diagram of the friction coefficient in the Reynolds number. As explained, the increase in the kinetic energy of the particles increases the shear stress of the tube surface and eventually increases the friction of the fluid with the inner surface of the tube. Similarly, with increasing Reynolds number, the turbulence and collapse of particles with the wall of the tube, due to kinetic energy, increases. The increase in the fluid with a volume percentage of 4% more than 2 %, and in the same way, 6% more than 4%, and 8% more than 6% is noticeable. The increase in nanoparticles of the fluid is the reason that increases the collision rate, leading to the increase in the friction coefficient of the particles with the wall and increase in the friction coefficient by increasing the Reynolds number at different viscosities.

Fig. 29 shows the Nusselt number diagram as a function of non-dimensioned length.

Table 2. Data values of different states of aluminum oxide nanofluid analysis at 4% volume fraction.

Percentage of change in thermal transfer coefficient rate	Geometry type
75% increase	Single injection
79% increase	Two injections in same direction
82% increase	Two injections with 90° angle
77% increase	Two injections with 180° angle
82.5% increase	Two injections of 90°, the second injection rate increases by 50%
81% increase	Two injections of 90°, the second injection rate decreases by 50%

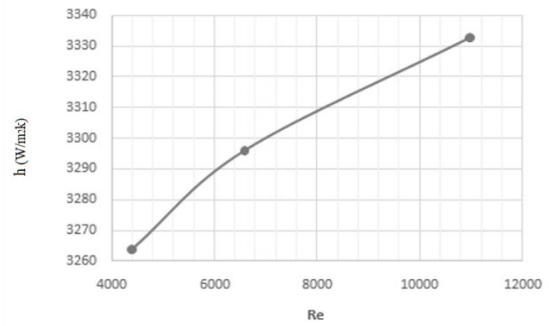


Fig. 27. Heat transfer coefficient diagram vs. Reynolds numbers for nanofluid of aluminum oxide with volume fraction of 0.04.

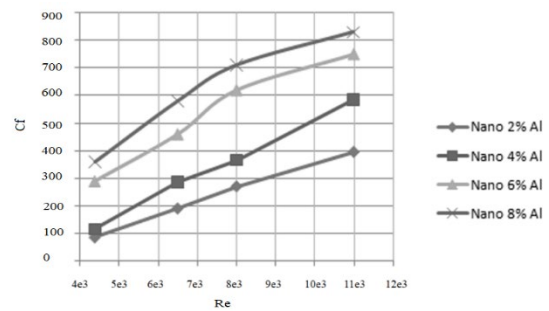


Fig. 28. Friction coefficient based on Reynolds number for different viscosities of nanofluid aluminum oxide.

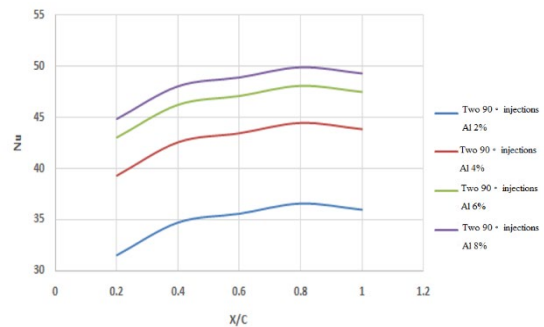


Fig. 29. Nusselt number diagram vs. tube length for different viscosities of aluminum oxide nanofluid.

The Nusselt number is a dimensionless parameter to represent the thermal criterion. Nusselt number is equal to:

$$Nu = \frac{hL}{k} \text{ or } \frac{hd}{k} \tag{5}$$

where h is the thermal transfer coefficient, l is the tube length, d is the diameter of the tube, and k is the thermal conductivity coefficient.

The Nu equation (Eq. (6)) shows the relationship between the Nusselt numbers as a function of Reynolds number for a volume fraction of 4%.

$$Nu = 9e^{-5} \times Re + 27.269 \quad (6)$$

In Fig. 29, it is seen that after injecting 2% aluminum oxide nanofluid, the curve starts to ascend. This is due to the effect of applying the momentum to the fluid and injecting the nanofluid into the base fluid, which disrupt the flow of fluid in the tube and also cause the boundary layer to disappear in the tube. The result is an increase in the collision of the nanofluid inside the base fluid, which increases the thermal transfer coefficient, and consequently, increases the thermal transfer rate and Nusselt number. The growing trend of other curves with volume fractions of 4, 6, and 8 is similar to the above, with the difference that increasing the viscosity of each is an influential factor on their greater ascending trend. An important point to express in completing the explanation of this section is that the nanofluid curves for the viscosities of 6% and 8% are close to each other. The reason is that each nanofluid has a capability to absorb and dissolve nanoparticles at a certain level and is saturated to a certain extent; however, a further increase in nanoparticles has no effects on the increase of the Nu and h numbers or the amount of thermal transfer.

To investigate the effect of injection and volume fraction on thermal transfer, the flow velocity at different sections, before and after each injection, is shown in Fig. 30. Positions 1 to 5 in the horizontal axis correspond to the after the first injection, after the second injection, after bending, after the third injection, and after the fourth injection, respectively. As can be seen, in the non-injection mode, the bending effect is shown as a velocity increase.

The shear stress of the flow with the tube causes a drop in velocity in the tube's length. These reliefs of speed drop by bending and injection are shown in Fig. 30. As can be seen, the effect of injection on the increase in speed is several times compared to bending. By increasing the volume fraction, it can be seen that the drop of velocity at different sections of the tube happens, which

the reason should be investigated in the increase of the friction of the flow in the tube.

As presented in Fig. 31, investigating different analyzed models shows that the effect of aluminum oxide nanofluid on the water is very effective on the Nusselt number, which is the evidence of the effectiveness of aluminum oxide nanofluid on the water during changing thermal transfer.

As shown in this figure, the changes in the thermal transfer rate cause greater Nusselt number indicating better performance of injection on the fluid compared to the non-injected mode. This is because applying the momentum to the output fluid from the injection jet and its collision with the fluid inside the tube causes an increase in the fluid velocity and eventually increases the thermal transfer rate and Nusselt number compared to other modes.

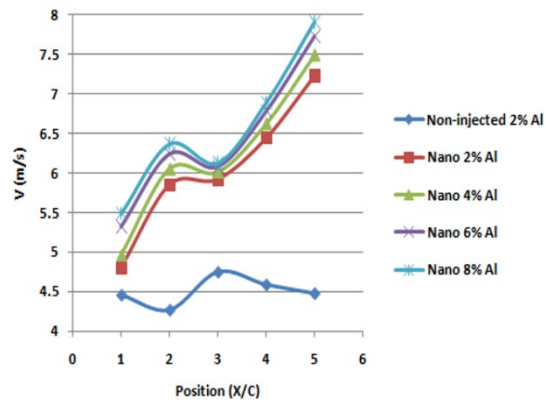


Fig. 30. Velocity diagram vs. position for different viscosities and non-injected mode.

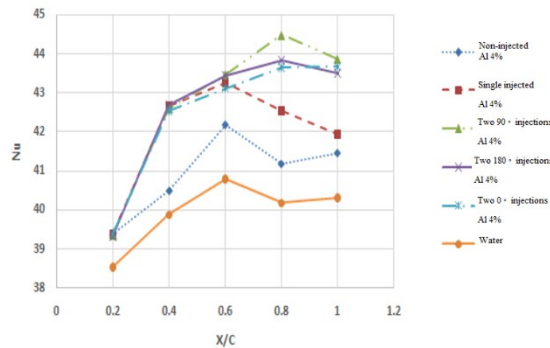


Fig. 31. Nusselt number diagram vs. the non-dimensioned positioning along the tube for different injection modes at 4% volume fraction for aluminum oxide nanofluid.

In other words, after the first injection, the fluid flows into the path of the tube and after a full round reaches its initial position of injection (zero-degree). In this situation, when the fluid loses lots of its kinetic energy and velocity begins to fall down in bending and increases its velocity, then in the middle of the way, at an angle of 90° to its initial injection mode, it is injected. This injection causes more increase in the velocity of the fluid to continue its path, and has better performance throughout the tube. In Fig. 32, the average values of Nusselt number are given as a function of different positions along the tube for different modes of injection of copper oxide nanofluid. It shows that the Nusselt number in the copper oxide nanofluid has an increase of 6% at a volume fraction of 4% compared to the aluminum oxide nanofluid (Fig. 31).

Fig. 32 also shows that the fluid containing copper oxide nanofluid has significant increases on the thermal transfer in comparison with the water, and for the two 90° injections mode, as described above for aluminum oxide nanofluid, it has the highest value.

In Fig. 33, the average values of Nusselt numbers, for the two nanofluids containing aluminum and copper oxides, are compared at a volume fraction of 4%. As expects, copper oxide has much higher Nusselt number values than aluminum oxide, so that for the non-injected copper oxide nanoparticles, its amounts are close to the aluminum oxide nanofluid with 90° injection. This indicates the importance of choosing nanoparticles. The same condition is shown in Fig. 34, which is presented at a volume fraction of 2%.

The point to note here is that, for a volume fraction of 4%, the difference in the Nusselt number of the copper oxide nanofluid is greater than that of the aluminum oxide nanofluid. The reason for this is that, with increasing volume fraction, the difference in the values for the two different analyzed nanoparticles is greater, so, copper oxide, which has a more and better thermal transfer power than aluminum oxide, shows more changes in thermal transfer rate and the value of Nusselt number by increasing volume fraction.

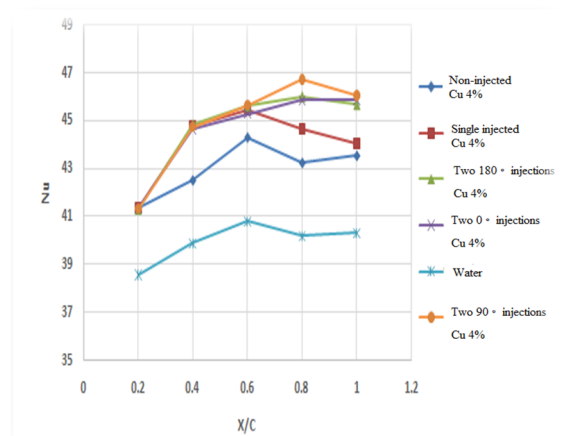


Fig. 32. Nusselt number diagram vs. the non-dimensional position along the tube for different injection modes at 4% volume fraction for copper oxide nanofluid.

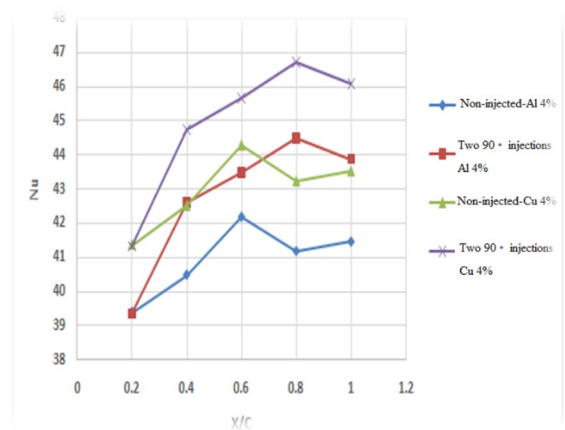


Fig. 33. Nusselt number diagram vs. the non-dimensional positioning along the tube for different injection modes at 4% volume fraction for two types of nanofluids.

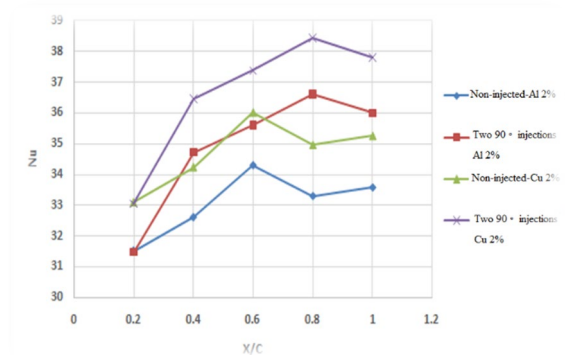


Fig. 34. Nusselt number diagram vs. the non-dimensional position along the tube for different injection modes at 2% volume fraction for two types of nanofluids.

4. Conclusions

In this paper, three-dimensional models of the spiral tube were investigated. Different turbulence models, injection position, etc. were investigated, which can be summarized in the following.

1. When the fluid reaches the place of the twist, due to the circulation of the fluid in the connection, a centrifugal force is created which forces the pressure near the outer tube to be greater than the pressure near the inner tube of the connection because of its more radius of curvature.

2. In the torsion of $\theta = 0$, is the maximum velocity to the inner part of the spiral tube (means the inner wall of the spiral tube). Because the surface of the outer wall is larger than the inner wall of the tube, and as a result, the force against the movement on the outer wall is more than the inner wall and the maximum velocity of movement moves towards the inner part of the connection wall.

3. Maximum kinetic energy of the turbulence occurs near the inner wall at the inlet of the twists and decreases by moving toward the outer wall and the connection outlet. Because shear stress near the inner wall is larger than the outer wall, most of the turbulent kinetic energy also occurs near the inner wall. This indicates that erosion and corrosion occur more often around the torsion internal tube.

4. In the torsion tubes, there is an increase in the thermal transfer compared to the direct tubes. The increase in the thermal transfer coefficient can be attributed to two mechanisms. First, centrifugal force due to the curvature of the tube, which produces a series of secondary vortex, flows at the curvature. This is the main cause of thermal transfer increases. Second, the current in the torsion tube, unlike the direct tubes, thermally cannot be considered a developed flow. Vortexes and return flows from the injection can have a great influence on the thermal and mass transfer.

5. The fluid injection causes the surface layer to collapse and develop, and it has a great influence on the structure of the flow field. Vortexes and return flows from the injection can have a great effect on the transfer of heat and mass

6. Nanofluids increase thermal conductivity by increasing the thermal conductivity coefficient.

7. As the volume fraction of nanoparticles increases, the heat transfer coefficient also increases.

8. For in-tube flows for modeling turbulence, the SST κ - ω model is the most suitable model for analyzing turbulence because it performs more accurate calculations in near-wall layers for flows that are associated with the phenomenon of separation and reciprocating pressure gradients. In addition, the equations have high sensitivity in free flows outside the boundary layer.

9. Increasing the inner diameter of the tube is the most suitable parameter for increasing the heat transfer coefficient.

10. Numerical modeling of a nanofluid in a one-phase manner using the empirical and numerical formulas obtained for their combined properties is an appropriate alternative for analyzing flow behavior in terms of its simplicity and accuracy.

11. In three different injection modes, the effect of two injections with a 90-degree angle is the best effect on injection action.

By analyzing different analytical models, it can be seen that the effect of Nano-fluid on water is very significant only on the average Nusselt number. For different injection modes, the coefficients of thermal transfer are given according to the different position of tube length for nanofluid containing aluminum oxide. It can be seen that compared to the non-injected mode, the thermal transfer values have increased significantly and for the two 90-degree injection mode, the highest value is obtained. The presence of an injection in the mid-tube compared to the initial injection in the ninety-degree mode causes the simultaneous effect of the bend and the two injections to increase the thermal transfer. In injection mode at zero and 180 degrees, due to the fact that the fluid faces the second injection after passing half a round, the thermal transfer rates are less and close to each other.

References

- [1] S. Hashemi and M. Akhavan-Behabadi, "An empirical study on heat transfer and

- pressure drop characteristics of CuO–base oil nanofluid flow in a horizontal helically coiled tube under constant heat flux”, *Int. Commun. Heat Mass Transf*, Vol. 39, No. 1, pp. 144–151, (2012).
- [2] M. A. Akhavan-Behabadi, M. F. Pakdaman and M. Ghazvini, “Experimental investigation on the convective heat transfer of nanofluid flow inside vertical helically coiled tubes under uniform wall temperature condition”, *International Communications in Heat and Mass Transfer*, Vol. 39, No. 4, pp. 556-564, (2012).
- [3] P. C. Mukesh Kumar, J. Kumar, S. Suresh and K. Praveen Babu, “Heat transfer enhancement in a helically coiled tube with Al₂O₃/water nanofluid under laminar flow condition”, *International Journal of Nanoscience*, Vol. 11, No. 5, pp. 1250029, (2012).
- [4] H. A. Mohammed and K. Narrein, “Thermal and hydraulic characteristics of nanofluid flow in a helically coiled tube heat exchanger”, *International Communications in Heat and Mass Transfer*, Vol. 39, No. 9, pp. 1375-1383, (2012).
- [5] K. Narrein and H. A. Mohammed, “Influence of nanofluids and rotation on helically coiled tube heat exchanger performance”, *Thermochimica Acta*, Vol. 564, pp. 13-23 (2013).
- [6] A. P. Sasmito, J. C. Kurnia and A. S. Mujumdar, “Numerical evaluation of laminar heat transfer enhancement in nanofluid flow in coiled square tubes”, *Nanoscale Research Letters*, Vol. 6, pp. 376, (2011).
- [7] A. S. Dalkilic, N. Kayaci, A. Celen, M. Tabatabaei, O. Yildiz, W. Daungthongsuk and S. Wongwises, "Forced convective heat transfer of nanofluids e a review of the recent literature", *Current Nanoscience*, Vol. 8, No. 6, pp. 949-969, (2012).
- [8] A. T. Akinshilo “Flow and heat transfer of nanofluid with injection through an expanding or contracting porous channel under magnetic force field”, *Engineering Science and Technology, an International Journal*, Vol. 21, No. 3, pp. 486-494, (2018).
- [9] S. M. S. Murshed, K. C. Leong and C. Yang, “A combined model for the effective thermal conductivity of nanofluids”, *Applied Thermal Engineering*, Vol. 29, No.11-12, pp. 2477-2483, (2009).
- [10] G. Huminic and A. Huminic, “Application of nanofluids in heat exchangers: a review”, *Renewable and Sustainable Energy Reviews*, Vol. 16, No. 8, pp. 5625-5638, (2012).
- [11] N. Kordani and A. Sadough, “Different Method to make Laminates by Shear Thickening Fluid”, *Science and Engineering of Composite Materials (SECM)*, Vol 21, No. 3, pp. 421-425, (2014).
- [12] F. Talati and A. A. Taheri, “Numerical study of induction heating by micro / nano magnetic particles in hyperthermia”, *Journal of Computational and Applied Research in Mechanical Engineering (JCARME)*, Vol. 9, No. 2, pp.259-273, (2020).
- [13] H. Baharvandi, P. Khaksari, M. Alebouyeh, M. Alizadeh, J. Khojasteh and N. Kordani, “Investigating the quasi-static puncture resistance of p-aramid nano composite impregnated with the shear thickening fluid”, *Journal of Reinforced Plastics and Composites*, Vol. 33, No. 22, pp. 2064-2072, (2014).
- [14] R. Taylor, S. Coulombe, T. Otanicar, P. Phelan, A. Gunawan, W. Lv, G. Rosengarten, R. Prasher and H. Tyagi, “Small particles, big impacts: a review of the diverse applications of nanofluids”, *Journal of Applied Physics*, Vol. 113, No. 1, pp. 011301, (2013).
- [15] A. Sergis and Y. Hardalupas, “Anomalous heat transfer modes of nanofluids: a review based on statistical analysis”, *Nanoscale Research Letters*, Vol. 6, pp. 391, (2011).
- [16] Y. Xuan and Q. Li, “Investigation on convective heat transfer and flow feature of nanofluids”, *ASME Journal of Heat*

- Transfer*, Vol. 125, No. 1, pp. 151-155, (2003).
- [17] E. V. Timofeeva, W. Yu, D. M. France, D. Singh and J. L. Routbort, "Nanofluids for heat transfer: an engineering approach", *Nanoscale Research Letters*, Vol. 6, pp. 182, (2011).
- [18] T. Srinivas and A. Venu Vinod, "Heat transfer intensification in a shell and helical coil heat exchanger using water-based nanofluids", *Chemical Engineering and Processing: Process Intensification*, Vol. 102, pp. 765-771, (2016).
- [19] E. Ebrahimnia Bajestan and H. Niazmand, "Flow and heat transfer of nanofluids with temperature dependent properties", *proceedings of the ASME 2010 "3rd Joint US-European Fluids Engineering Summer Meeting"* and "8th International Conference on Nanochannels, Microchannels, and Minichannels", Montreal, Canada, pp. 733-739, (2010).
- [20] U. Rea, T. McKrell, L. Hu and J. Buongiorno, "Laminar convective heat transfer and viscous pressure loss of alumina-water and zirconia-water nanofluids", *International Journal of Heat and Mass Transfer*, Vol. 52, No. 7-8, pp. 2042-2048, (2009).
- [21] A. V. Kuznetsov and D. A. Nield, "Natural convective boundary-layer flow of a nanofluid past a vertical plate", *International Journal of Thermal Sciences*, Vol. 67, No. 2, 239-246, (2010).
- [22] A. Noghrehabadi, M. Ghalambaz and A. Ghanbarzadeh, "Effects of Variable Viscosity and Thermal Conductivity on Natural-Convection of Nanofluids Past a Vertical Plate in Porous Media", *Journal of Mechanics*, Vol. 33, No. 3, pp. 320-328, (2014).
- [23] Y. Xuan and Q. Li, "Heat transfer enhancement of nanofluids, Int J Heat Fluid Flow", *International Journal of Heat and Fluid Flow*, Vol. 21, No. 1, pp. 58-64, (2000).
- [24] Y. Xuan, Q. Li and W. Hu, "Aggregation structure and thermal conductivity of nanofluids", *American Institute of Chemical Engineers*, Vol. 49, No. 4, pp. 1038-1043, (2003).
- [25] G. Sheikhzadeh, M. Mollamahdi and M. Abbaszadeh, "Analytical study of flow field and heat transfer of a non-Newtonian fluid in an axisymmetric channel with a permeable wall", *Journal of Computational and Applied Research in Mechanical Engineering (JCARME)*, Vol. 7, No. 2, pp. 161-173, (2018).
- [26] M. Sh. Mazidi, M. Alizadeh, L. Nourpour and V. Shojaee Shal, "Estimating the unknown heat flux on the wall of a heat exchanger internal tube using inverse method", *Journal of Computational and Applied Research in Mechanical Engineering (JCARME)*, Vol. 5, No. 5, pp. 127-136, (2016).
- [27] S. M. Fotokian and M. Nasr Esfahany, "Experimental investigation of turbulent heat transfer of γ -Al₂O₃ water nanofluid in circular tube", *International Journal of Heat and Fluid Flow*, Vol. 28, No. 2, pp. 203-210, (2007).
- [28] S. Zeinali Heris, Taofik H. Nassan, S. H. Noie, H. Sardarabadi and M. Sardarabadi, "Laminar convective heat transfer of Al₂O₃/water nanofluid through square cross-sectional duct", *International Journal of Heat and Fluid Flow*, Vol. 44, pp. 526-534, (2013).
- [29] Mohamed H. Shedid, "Computational Heat Transfer for Nanofluids through an Annular Tube", *Proceedings of International Conference on Heat Transfer and Fluid Flow*, Prague, Czech Republic, August 11-12, No. 206, pp. 1-10, (2014).
- [30] J. Choi and Y. Zhang, "Numerical simulation of laminar forced convection heat transfer of Al₂O₃-water nanofluid in a tube with return bend", *International Journal of Thermal Sciences*, Vol. 55, pp. 90-102, (2012).
- [31] W. Williams, J. Buongiorno and L.W. Hu, "Experimental investigation of turbulent convective heat transfer and pressure loss of alumina/water and zirconia/water nanoparticle colloids (nanofluids) in

- horizontal tubes”, *ASME Journal of Heat Transfer*, Vol. 130, No. 4, pp. 042412-042419, (2008).
- [32] Z. Wu, L. Wang and B. Sundén, “Pressure drop and convective heat transfer of water and nanofluids in a double-tube helical heat exchanger”, *Applied Thermal Engineering*, Vol. 60, No. 1-2, pp. 266-274, (2013).
- [33] D. J. Gunn, “Experimental investigation of Transfer Heat or Mass to Particles in Fixed and Fluidized Beds”, *Int. J. Heat Mass Transfer*, Vol. 21, No. 4, pp. 467-476, (1978).
- [34] F. Hormozi, B. Zare Nezhad and H. R. Allahyar, “An experimental investigation on the effects of surfactants on the thermal performance of hybrid nanofluids in helical coil heat exchangers”, *International Communications in Heat and Mass Transfer*, Vol. 78, pp. 544-553, (2016).
- [35] N. Putra, W. Roetzel and S.K. Das, “Natural convection of nanofluids”, *Heat and Mass Transfer*, Vol. 39, No. 8-9, pp. 775-786, (2003).

How to cite this paper:

Hamid Zalnezhad, and N. Kordani, “ Numerical analysis of heat transfer in helical tube with the aluminum oxide Al_2O_3 nanofluid injection in water”, *Journal of Computational and Applied Research in Mechanical Engineering*, Vol. 10, No. 1, pp. 211-227, (2020).

DOI: 10.22061/jcarme.2019.3798.1444

URL: http://jcarme.sru.ac.ir/?_action=showPDF&article=1055

